A Single-Coupling Approach to Wireless Power Transfer and Communication

Ujwala P. Ghude[1], Ganesh G. Mhatre[2]
[1]M.E Student, [2]Assistant professor
[1]Yadavrao Tasgaonkar Institute of Engineering and Technology, Chandhai, India
[2]New Horizon Institute of Technology and Management, Thane, India
[1]upghudeo6@gmail.com, [2]ganeshmha@gmail.com

***Abstract*-This article presents a method for simultaneous WPT and full-duplex communication (FDC) using a pair of coupling coils. Power transfer is achieved through a double-sided LCC compensation network, while a four-resonance dual-rejection (FRDR) structure enables bidirectional data transmission. The proposed topology ensures that the circuits on each side not only transmit and receive intended data carriers but also suppress interference from unwanted carriers. Rated power transfer is maintained with minimal degradation, ensuring reliable operation during simultaneous power and data exchange. A systematic parameter design methodology is presented, along with an analysis of interference between power waves and data carriers and crosstalk among multiple data channels. A prototype system validates the feasibility of the proposed approach, demonstrating 600 W power transfers with a concurrent data rate of 80 kbps.**

***Index Terms*- Wireless Power Transfer, full-duplex communication (FDC), four-resonance dual-rejection.**

I. INTRODUCTION

The last few decades have seen a surge in interest in WPT innovation as a result of its potential uses in EVs, rotary machinery, electronic goods, medicinal surgical devices, and domestic gadgets that require the transfer of electrical energy without human contact [1-2]. For these applications, reliable real-time communication between the primary and secondary sides is crucial to improve efficiency, control, and operational stability. Conventional communication technologies such as Bluetooth, ZigBee, Wi-Fi, and RF have been used in WPT systems; however, these require complex pairing processes and often exhibit transmission delays [3]. To overcome such limitations, researchers have investigated the incorporation of power and data transfer (DT) into a unified WPT framework. These methods offer economic benefits, reduced system complexity, and elimination of additional cabling, making them particularly suitable for compact and constrained environments.

A widely studied approach involves utilizing the inherent power transfer channel (PTC) for data transmission [4]. Such schemes are advantageous for robotic joints and implantable medical devices, where flexibility and reduced hardware are critical. Existing methods typically include: (i) modulating the power carrier to transmit data [5], and (ii) employing a single dedicated data carrier [6-7]. However, modulating the power carrier compromises transfer efficiency and limits data rates due to the low frequency of the carrier, while most schemes allow only half-duplex communication. Recent advances have demonstrated FDC through QPSK [8] and FSK with partial coupling coils [9-10]. While effective, these solutions require sophisticated modulation/demodulation circuits, raising system cost and limiting applicability in low-cost applications.

This paper introduces a novel approach to achieve simultaneous WPT and full-duplex communication using simple passive LC components. The proposed system constructs serial and parallel LC networks, which form a FRDR structure. Amplitude shift keying (ASK) is employed for data transfer, enabling cost-effective implementation with minimal circuitry, such as an analog switch. Two equivalent S–S compensation topologies are used to carry dual data channels while preserving efficient power transfer. This design achieves low-cost, flexible, and reliable simultaneous WP and DT.

II. COMMUNICATION

The illustrated FRDR configuration and its corresponding frequency response are presented in Fig. 1. The configuration comprises two parallel LC networks, specifically L_{p1}, C_{p1} and L_{p2}, C_{p2}, along with a series LC network, denoted as L_1, C_{s1}. where L_{p1}, C_{p1}, L_{p2}, and C_{p2} fulfil the conditions $1= \omega_{p1}^2 L_{p1} C_{p1} = \omega_{p2}^2 L_{p2} C_{p2}$ and $\omega p2 > \omega p1$. In order to facilitate the simultaneous transfer of two data carriers, it is essential to adjust two resonance points of the FRDR structure so that they align with its corresponding rejection points. This indicates that a resonance point from one branch coincides precisely with the rejection point of the other branch.

Fig. 2 illustrates the configuration of the proposed method. The configuration includes four parallel LC networks), two series LC networks, two sampling resistors, and two alternating current signal sources (AC1, AC_2). The angular frequencies for AC_1 and AC_2 are denoted as ω_1 and ω_2, respectively.

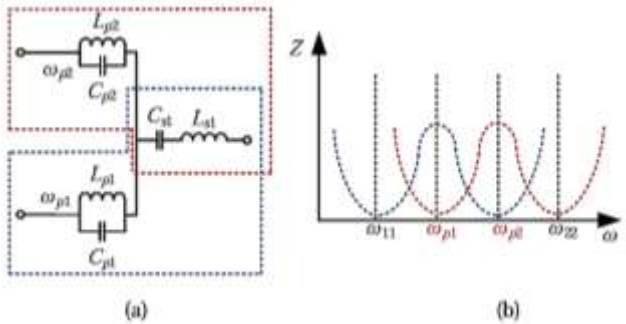

(a) (b)

Fig. 1. (a) FRDR & (b) frequency response

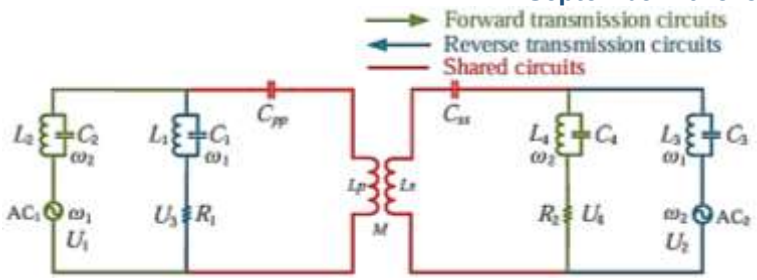

Fig. 2 Proposed FDC channel

The f_r of LCC methodology is solely determined by the inductances and capacitances, remaining unaffected by coupling and load conditions. In contrast to the S-S compensation topology, the power transferred, along with the i/p & o/p currents, exhibits a proportional relationship to the mutual inductance M [11]. Providing excellent layout versatility, the network can keep the coil's initial current stable and the supplementary output current constant. b) Adding to that, a lot of the high-order harmonics that come out of the main inverter and secondary rectifier are filtered out by the series L and parallel C on both sides. This filtering greatly improves the signal-to-noise ratio and reduces harmonic interference, making it ideal for data transmission. Different kinds of WPT can also benefit from the proposed strategy. The comprehensive system's schematic structure is shown in Fig. 3.

Edc serves as the input DC voltage source. The FBI is composed of four MOSFETs, designated as S1 through S4. (Lp, Cp, Lf1, Cf1) and (L, Cs, Lf2, Cf2) represent the fundamental components of the LCC. the resonant tank and the secondary LCC resonant tank, respectively. (Lr1, Cr1), (Lr2, Cr2), (Lr3, Cr3), and (Lr4, Cr4) represent the wave trappers on both the primary and secondary sides, and they fulfil the necessary conditions. For the purpose of streamlining the analysis, it is posited that Lr1 is equal to Lr3 and Lr2 is equal to Lr4. [12].

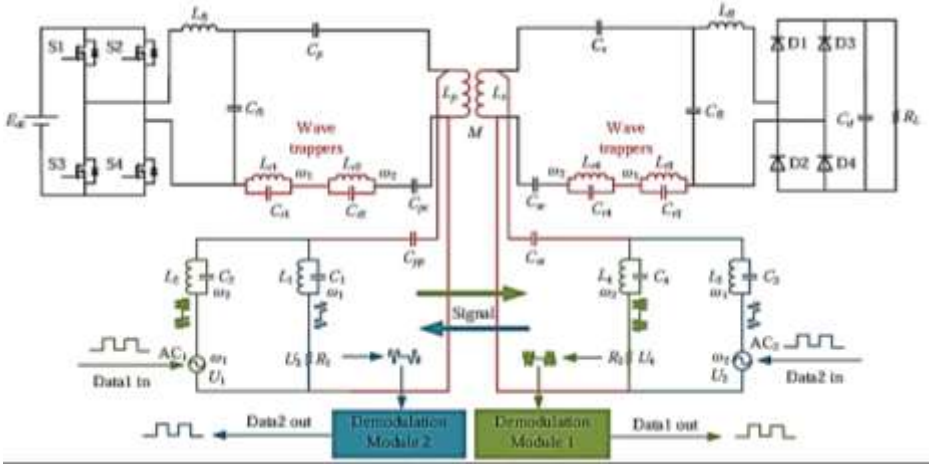

Fig. 3 WPS circuit

C_{pc} and C_{sc} are utilised in this study to mitigate the inductance associated with the power wave caused by the inclusion of wave trappers, ensuring that power transfer remains unaffected. The inclusion of these two compensation C allows for a reduction in the necessity for a very small L value in the trapper, thereby facilitating the attainment of higher impedance in the trappers. In fact, the primary and secondary resonant C_p and Cs can be substituted with C_{peq} and C_{seq}, respectively, leading to their elimination.

Energy Transmission During the operation of the FBI, the DTCs exhibit high impedance, effectively behaving as open circuits, while the wave tappers function as L. Additionally, the L are balanced by C that are connected in series. Consequently, the PTC can be regarded as analogous to the initial double-sided LCC configuration in the WPT system. Fig. 4 illustrates the equivalent network of the PT channel. In this context, U_{ac} represents the output voltage generated by the FBI, while R_{eq} denotes the Req associated with both the rectifier and the load RL. According to reference [13], the R of the Req. is defined by the equation $R_{eq} = \frac{8R_L}{\pi^2}$.

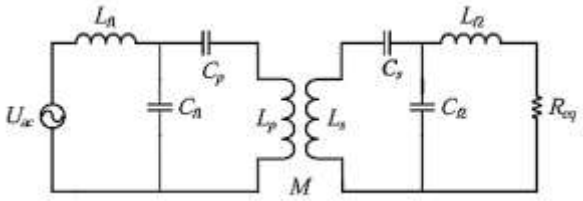

Fig. 4 Equivalent circuit

Given that ω_1 is greater than ω_2, when data is forwarded, the parallel network constituted by (L_2, C_2) and (L_4, C_4) functions as C, allowing for the derivation of the capacitance of the equivalent C.

$$C_{eq_1} = C_2 - \frac{1}{\omega_1^2 L_2} = C_4 - \frac{1}{\omega_1^2 L_4} \qquad (1)$$

In order to achieve resonance in the primary and secondary circuits at the ω_1, the series configurations consisting of (L_p, C_{pp}) and (L, C_{ss}) must function as L at this specific angular frequency ω1. The Leq may be determined.

$$L_{eqv_1} = L_p - \frac{1}{\omega_1^2 C_{pp}} = L_s - \frac{1}{\omega_1^2 C_{ss}} = \frac{1}{\omega_1^2 C_{eqv_1}} \quad (2)$$

In a manner akin to forward transmission, the parallel configurations established by (L_1, C_1) and (L_3, C_3) function as L, allowing for the derivation of the L of the equivalent L.

$$L_{eqv_2} = \frac{L_1}{1-\omega_2^2 L_1 C_1} = \frac{L_3}{1-\omega_2^2 L_3 C_3} \quad (3)$$

The C of the equivalent C in the series configurations created by (Lp, Cpp) and (L, Css) can be determined.

$$C_{eqv_2} = \frac{C_{pp}}{1-\omega_2^2 L_p C_{pp}} = \frac{C_{ss}}{1-\omega_2^2 L_s C_{ss}} = \frac{1}{\omega_2^2 L_{eqv_2}} \quad (4)$$

III. SYSTEM PARAMETER DESIGN

System variables are capable of being configured according to the procedures depicted in Fig. 5. During the design phase, the frequencies of the two data carriers (i.e., ω_1 and ω_2), along with L1 and Lp, can be established in advance, allowing for the derivation of C_1 and C_3.

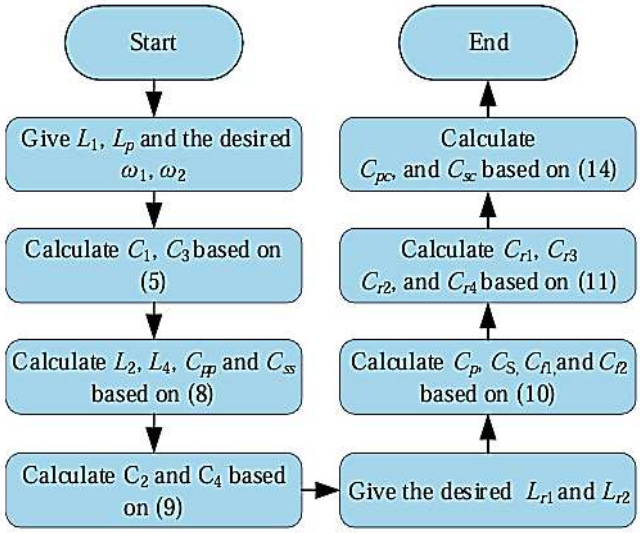

Fig. 5 Diagram illustrating the design parameters

$$C_1 = C_3 = \frac{1}{\omega_1^2 L_1} = \frac{1}{\omega_1^2 L_3} \quad (5)$$

Based on references (1) and (2), it can be concluded that

$$L_{eqv_1} = L_p - \frac{1}{\omega_1^2 C_{pp}} = L_s - \frac{1}{\omega_1^2 C_{ss}} = \frac{1}{\omega_1^2\left(C_2 - \frac{1}{\omega_1^2 L_2}\right)} = \frac{1}{\omega_1^2\left(C_4 - \frac{1}{\omega_1^2 L_4}\right)} \quad (6)$$

Based on references (3) and (4), it can be concluded that

$$C_{eqv_2} = \frac{C_{pp}}{1-\omega_2^2 L_p C_{pp}} = \frac{C_{ss}}{1-\omega_2^2 L_s C_{ss}} = \frac{1}{\omega_2^2\left(\frac{L_1}{1-\omega_2^2 L_1 C_1}\right)} = \frac{1}{\omega_2^2\left(\frac{L_3}{1-\omega_2^2 L_3 C_3}\right)} \quad (7)$$

By integrating equations (6) and (7), the subsequent equations can be derived.

$$\begin{cases} L_2 = L_4 = \dfrac{L_p\left(\omega_1^4 + \omega_2^4\right) - \omega_1^2\omega_2^2\left(L_1 + 2L_p\right)}{\omega_1^2\omega_2^2} \\ C_{pp} = C_{ss} = \dfrac{\omega_1^2 - \omega_2^2}{\omega_2^2\left(\left(L_1 + Lp\right)\omega_1^2 - L_p\omega_2^2\right)} \end{cases} \quad (8)$$

From the analysis presented in (8), it follows that

$$C_2 = C_4 = \frac{1}{\omega_2^2 L_2} = \frac{1}{\omega_2^2 L_4} = \frac{\omega_1^2}{L_p\left(\omega_1^4 + \omega_2^4\right) - \omega_1^2\omega_2^2\left(L_1 + 2L_p\right)} \quad (9)$$

The operational angular frequency of the FBI is defined as ωr =2πfr. In the context of a double-side LCC type WPT system, the components C_p, C_s, C_{f1}, and C_{f2} must satisfy the following conditions.

$$\begin{cases} C_p = \dfrac{1}{\omega_r^2(L_p - L_{f1})} \\ C_s = \dfrac{1}{\omega_r^2(L_s - L_{f2})} \\ C_{f1} = \dfrac{1}{\omega_r^2 L_{f1}} \\ C_{f2} = \dfrac{1}{\omega_r^2 L_{f2}} \end{cases} \quad (10)$$

IV. RESULTS AND DISCUSSION

In order to confirm the effectiveness of the suggested method, accordance with Fig. 3 The data transceiver employs for the generation of sinusoidal data carriers, while also managing the analog switch (ADG5419) for the modulation.

ASK as well as LSK represent the predominant techniques utilized for data modulation in the context of DT [14]. OOK can be considered a specific instance of ASK, which is extensively utilized in signal modulation. The primary benefit of ASK as well as LSK lies in their straightforward nature.

Table 1 System Parameter

Parameter	Value	Parameter	Value
E_{dc}	100 V	f_r	85 kHz
L_p, L_s	60.6 μH	C_p	86.4 nF
L_{f1}	20 μH	C_r	70.7 nF
L_{f2}	11 μH	C_{f1}	175.3 nF
L_{r1}, L_{r3}	30 μH	C_{f2}	318.7 nF
L_{r2}, L_{r4}	30 μH	C_{r1}, C_{r3}	211 pF
C_{pp}, C_{ss}	58.4 nF	C_{r2}, C_{r4}	586 pF
L_1, L_3	22 μH	U_1, U_2	13 V(pk)
f_1	2 MHz	C_1, C_3	287.8 pF
L_2, L_4	47 μH	f_2	1.2 MHz
C_{pp}, C_{ss}	185 pF	C_2, C_4	374 pF
R_1	470 Ω	M	18 μH
R_L	4.85 Ω	R_3	470 Ω

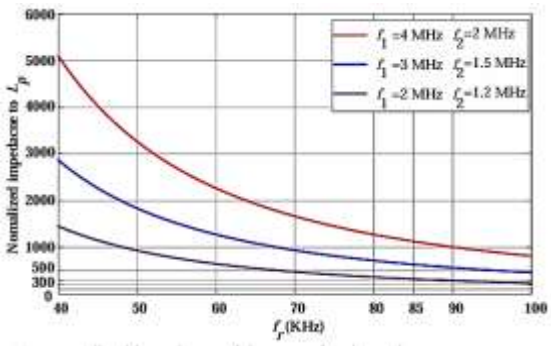

Fig. 6. Z_{normal} of DTC to Lp.

As the DTC exhibits significant Z to power waves and can be regarded as open circuits. Given the parameters L_1=22 uH, L_2=47 uH, R_1=470 Ω, and three sets of ω_1 and ω_2 , as the fs of the inverter fr transitions from 40 kHz to 100 kHz, the normalized impedance curves relative to Lp can be represented as shown in Fig. 6. Fig. 6 illustrates that a) When it comes to the P wave, the DT module's impedance is far higher than Lp's. b) As the proportion of the signal wave's f to the P wave's frequency increases, the DT channel's Z also increases. Elevated Z levels are correlated with a rising ratio.

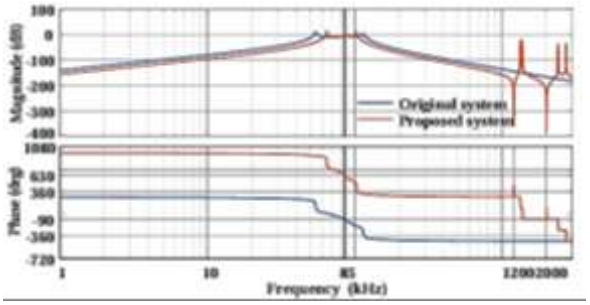

Fig. 7. Bode plots illustrating the characteristics of the PTC with a load resistance of 4.85 Ω.

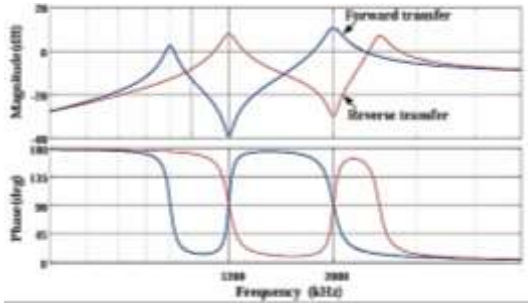

Fig. 8. Bode plots of DTCs

Fig.7 illustrates the Bode plots corresponding to the PTC. Analysis of Fig. 7indicates that the power channel gains remain consistent before and after the incorporation of the trappers at the switching frequency of the FBI. The power transfer at the inverter's switching frequency remains largely unchanged despite the inclusion of the DT channel.

In order to evaluate the responses of DTC, the Bode plots are illustrated as shown in Fig. 8. As illustrated in Fig. 8, the forward transfer channel demonstrates the capability to obstruct the data carrier at 1.2 MHz while simultaneously allowing the passage of the data carrier at 2 MHz's the RTC operates in an opposite manner. Consequently, FDC can be realized, contingent upon the responses of DTC.

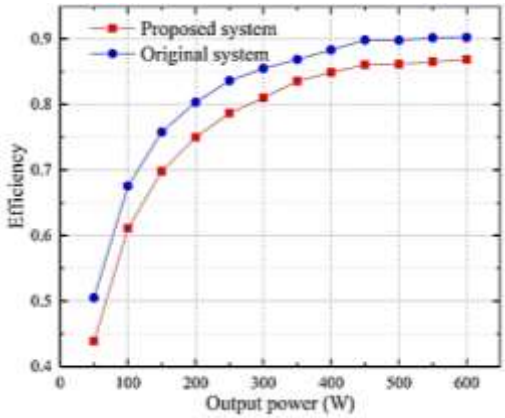

Fig. 9. Effectiveness of the energy transmission pathway

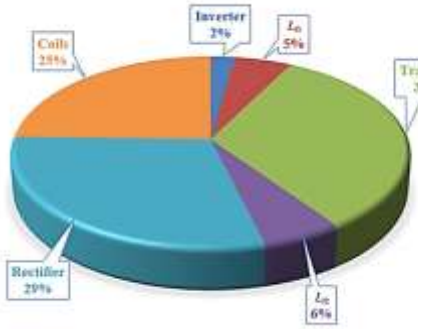

Fig. 10 Power losses distribution

Fig. 9 illustrates the efficiency of the DC-DC PTC, comparing scenarios with and without trappers. The inclusion of trappers in the PTC results in a noticeable decrease in the efficiency of the channel. The assessment of the Suggested method performance involves measuring power losses, which encompass inverter loss, L loss, coil loss, trapper loss, and rectifier loss. The distribution of these P_L is illustrated in Fig. 10. Fig. 10 illustrates that the power loss attributed to trappers constitutes a significant portion, as the internal resistances of the L within the trappers are comparatively elevated. In this, the R_{int} of each L, measured at the f_P, is recorded at 0.1 Ω.

To enhance the effectiveness of the suggested method, several strategies may be implemented, including the optimisation of parameters, the use of L with elevated Q values, and the incorporation of parallel dual-rejection trappers. To mitigate the power losses induced by the trappers, incorporation of the two trappers into coupling coils is also feasible. Nonetheless, the interaction between coils will require additional examination in subsequent studies.

V. CONCLUSION

A method for simultaneous and PT in WPT systems is presented in this article. The study validates the viability of this method. The attributes in the networks are employed to establish three distinct transfer channels. Two data carriers are modulated using amplitude shift keying and transmitted alongside the power carrier through a single coupling interface. Additionally, this document examines the functioning of the system and the interactions between PT and DT.

The findings demonstrate that data can be transmitted in both directions concurrently at a baud rate of 80 kbps. Although the introduction of trappers results in power loss, the proposed method offers an innovative approach to enable full duplex communication within WPT systems.

REFERENCES

[1] W. Zhang and C. C. Mi, "Compensation Topologies of High-Power Wireless Power Transfer Systems," in IEEE Transactions on Vehicular Technology, vol. 65, no. 6, pp. 4768-4778, June 2016.

[2] Li, Y., et al., A New Coil Structure and Its Optimization Design with Constant Output Voltage and Constant Output Current for Electric Vehicle Dynamic Wireless Charging. IEEE Transactions on Industrial Informatics, 2019. 15(9): p. 5244-5256.

[3] Song, K., et al., A Rotation-Lightweight Wireless Power Transfer System for Solar Wing Driving. IEEE Transactions on Power Electronics, 2019. 34(9): p. 8816-8830.

[4] Li, Y., et al., Analysis, Design, and Experimental Verification of a Mixed High-Order Compensations-Based WPT System with Constant Current Outputs for Driving Multistring LEDs. IEEE Transactions on Industrial Electronics, 2020. 67(1): p. 203-213.

[5] X. Li, C. Tang, X. Dai, P. Deng and Y. Su, "An Inductive and Capacitive Combined Parallel Transmission of Power and Data for Wireless Power Transfer Systems," in IEEE Transactions on Power Electronics, vol. 33, no. 6, pp. 4980-4991, June 2018.

[6] L. Ji, L. Wang, C. Liao and S. Li, "Simultaneous Wireless Power and Bidirectional Information Transmission With a Single-Coil, Dual Resonant Structure," in IEEE Transactions on Industrial Electronics, vol. 66, no. 5, pp. 4013-4022, May 2019.

[7] C. Huang, C. Lin, and Y.Wu, "Simultaneous wireless power/data transfer for electric vehicle charging," IEEE Trans. Ind. Electron., vol. 64, no. 1, pp. 682–690, Jan 2017.

[8] Y. Sun, P. Yan, Z. Wang and Y. Luan, "The Parallel Transmission of Power and Data With the Shared Channel for an Inductive Power Transfer System," in IEEE Transactions on Power Electronics, vol. 31, no. 8, pp. 5495-5502, Aug. 2016.

[9] J. Wu, C. Zhao, Z. Lin, J. Du, Y. Hu, and X. He, "Wireless power and data transfer via a common inductive link using frequency division multiplexing," IEEE Trans. Ind. Electron., vol. 62, no. 12, pp. 7810 7820,Jul. 2015.

[10] Z. Qian, R. Yan, J. Wu and X. He, "Full-Duplex High-Speed Simultaneous Communication Technology for Wireless EV Charging," in IEEE Transactions on Power Electronics, vol. 34, no. 10, pp. 9369-9373, Oct. 2019.
[11] Y. Yao, H. Cheng, Y. Wang, J. Mai, K. Lu and D. Xu, "An FDM-based Simultaneous Wireless Power and Data Transfer System Functioning with High-rate Full-duplex Communication," in IEEE Transactions on Industrial Informatics. doi: 10.1109/TII.2020.2967023
[12] W. Li, H. Zhao, J. Deng, S. Li and C. C. Mi, "Comparison Study on SS and Double-Sided LCC Compensation Topologies for EV/PHEV Wireless Chargers," in IEEE Transactions on Vehicular Technology, vol. 65, no. 6, pp. 4429-4439, June 2016.
[13] J. Moon, H. Hwang, B. Jo, H. Shin and S. Kim, "Design of a 5-W power receiver for 6.78 MHz resonant wireless power transfer system with power supply switching circuit," in IEEE Transactions on Consumer Electronics, vol. 62, no. 4, pp. 349-354, November 2016.
[14] I. A. Mashhadi, M. Pahlevani, S. Hor, H. Pahlevani and E. Adib, "A New Wireless Power-Transfer Circuit for Retinal Prosthesis," in IEEE Transactions on Power Electronics, vol. 34, no. 7, pp. 6425-6439, July 2019.